Natural iron fertilization by shallow hydrothermal sources fuels diazotroph blooms in the Ocean

Authors: Sophie Bonnet[1], Cécile Guieu[2], Vincent Taillandier[2], Cédric Boulart[3], Pascale Bouruet-Aubertot[4], Frédéric Gazeau[2], Matthieu Bressac[2], Angela N. Knapp[5], Yannis Cuypers[4], David González-Santana[6,7], Heather J. Forrer[5], Jean-Michel Grisoni[2], Olivier Grosso[1], Jérémie Habasque[6], Mercedes Jardin-Camps[1], Nathalie Leblond[2], Frédéric Le Moigne[1], Anne Lebourges-Dhaussy[6], Caroline Lory[1], Sandra Nunige[1], Elvira Pulido-Villena[1], Andrea L. Rizzo[9,10], Géraldine Sarthou[6], Chloé Tilliette[2]

Affiliations:
[1]Mediterranean Institute of Oceanography, Aix Marseille Université, Université de Toulon, CNRS, IRD, MIO UM 110, 13288, Marseille, France
[2]Laboratoire d'Océanographie de Villefranche, Institut de la Mer de Villefranche, CNRS, Sorbonne Université, 06230 Villefranche-sur-Mer, France
[3]Adaptation et Diversité en Milieu Marin, UMR 7144 AD2M CNRS-Sorbonne Université, Station Biologique de Roscoff, 29680 Roscoff, France
[4]Laboratoire d'Océanographie et du Climat: Expérimentation et Approches Numériques (LOCEAN-IPSL), Sorbonne University, CNRS-IRD-MNHN, 75005 Paris, France
[5]Florida State University, Department of Earth, Ocean, and Atmospheric Sciences, Tallahassee, Florida, 32306, USA
[6]Laboratoire des Sciences de l'Environnement Marin LEMAR, CNRS, Univ Brest, IRD, Ifremer, F-29280 Plouzane, France
[7]Instituto de Oceanografía y Cambio Global, IOCAG, Universidad de Las Palmas de Gran Canaria, 35017
[8]Institut de la Mer de Villefranche, IMEV, Sorbonne Université, Villefranche sur Mer
[9]Istituto Nazionale di Geofisica e Vulcanologia, Sezione di Palermo, Via Ugo La Malfa 153, 90146 Palermo, Italy
[10]Istituto Nazionale di Geofisica e Vulcanologia, Sezione di Milano, Via Alfonso Corti 12, 20133 Milano, Italy

***Correspondence to:** sophie.bonnet@mio.osupytheas.fr, cecile.guieu@imev-mer.fr

Abstract. Iron is an essential nutrient, regulating productivity in ~30% of the ocean. Compared to deep (>2000 m) hydrothermal activity at mid-ocean ridges that provide iron to the ocean's interior, shallow (<500 m) hydrothermal fluids are likely to influence the surface's ecosystem. However, their effect is unknown. Here we show that fluids emitted along the Tonga volcanic Arc (South Pacific) have a dramatic impact on iron concentrations in the photic layer through vertical diffusion. This enrichment stimulates biological activity, resulting in an extensive patch of chlorophyll. Diazotroph activity is 2-8 times higher, and carbon export fluxes 2-3 times, compared to adjacent unfertilized waters. Such findings reveal a novel mechanism of natural iron fertilization in the ocean, fueling regional hot spot sinks for atmospheric CO_2.

One-Sentence Summary: Shallow hydrothermal iron fertilizes the overlying surface ocean creating an oasis in the desert

Main Text (2500 words). Atmospheric dinitrogen (N_2) fixed by diazotrophs provides the largest external source of new N to the surface ocean, supporting food webs and organic matter export in 60% of our oceans[1, 2]. However, diazotrophs face a major challenge: besides phosphorus requirements, the iron (Fe)-rich nitrogenase enzyme that catalyzes N_2 fixation imposes a high Fe demand, but its bioavailability in the ocean often limits the growth of these organisms[2, 3]. The Western subtropical South Pacific (WTSP) is a recognized hotspot of N_2 fixation activity, with an estimated contribution of ~21% to the global fixed N input[4]. Fe supply through atmospheric deposition is known to control large-scale diazotroph biogeography[5], but such aeolian inputs are extremely low in this remote region[6], suggesting the presence of alternative Fe fertilization processes underlying this ecological success. Identifying these mechanisms is of the utmost importance as diazotrophs have recently been identified as key drivers of future marine net primary productivity in response to climate change[7].

The seafloor of the WTSP hosts the Tonga-Kermadec subduction zone, stretching 2,500 km from New Zealand to Tonga (Fig. 1A). It is the fastest converging, most seismically active subduction zone, with the highest density of underwater volcanic centers on Earth[8]. These systems are associated with extensive plumes of ^{3}He in the bathypelagic ocean (1500-2000 m) that fingerprint deep hydrothermal sources originating in the Lau basin[9, 10]. Massoth et al.[11] also identified shallower sources (<500 m) along the Tonga arc, associated with significantly elevated dissolved Fe (DFe) and manganese (DMn) concentrations close to the seafloor. Guieu et al.[6] demonstrated that these shallow sources were able to bring DFe up to the photic layer (~100 m) at high concentrations (up to 66 nmol liter^{-1}). These Fe infusions are hypothesized to fuel the observed N_2 fixation hot spot associated with an elevated chlorophyll patch persisting 6 months per year in this region[4, 6] (Fig 2A,B). Yet, there is currently no empirical evidence of the direct effect of such hydrothermal Fe fertilization on the overlying planktonic ecosystem, with the implication that a significant part of new N entering the tropical Pacific -thanks to hydrothermal Fe- is likely missing from N budgets. Such an Fe supply mechanism would challenge the prevailing paradigm that diazotroph productivity is mainly mediated by Fe from desert dust deposition[5] in N-limited regions.

Here, we combine acoustic, chemical, physical, and biological data acquired during the TONGA expedition (GEOTRACES GPpr14, November 2019, https://doi.org/10.17600/18000884) to document the mechanistic link between Fe supply from submarine volcanism and the response of the surface plankton community. We bring together multiple observations from a zonal transect between the Tonga volcanic Arc and the South Pacific Gyre, which serves as a reference deep-sea site where the ocean surface is not impacted by hydrothermal activity. We demonstrate that Fe-rich fluids emitted by shallow hydrothermal venting directly fertilize the overlying surface ecosystem, inducing enhanced biological biomass and carbon export fluxes mostly due to the activity of N_2 fixing microbes.

The targeted submarine volcano (Volcano #1[11]) is a large stratovolcano (basal diameter 28 km) located in the central part of the Tonga Arc (21°9.273'S; 175°44.664'W) (Fig. 1A). Strong continuous acoustic plumes were observed rising from the sea floor (195 m depth) up to ~30 m below the surface (Fig. 1B). These plumes were also associated with intense gas bubble emissions (Fig. 1C) and strong anomalies in pH, turbidity, and redox potential (Eh) (Fig. 1D) from the seafloor up to ~160 m. Methane concentrations that reached >100 nmol liter^{-1} (Fig. 1E) and the excess of ^{3}He and ^{4}He concentrations (Fig. S1) confirmed the hydrothermal origin of the plumes.

DFe and DMn were enriched ~80-fold in the hydrothermal waters above Volcano #1 (Fig. 1E) compared to similar depths in the WTSP[6, 12]. DFe and CH_4 concentrations were positively correlated together (R^2=0.89, p<0.05). DFe reached concentrations as high as 48.5 nmol $liter^{-1}$ at 195 m (within the main acoustic signal), and although they decreased towards the surface, elevated DFe concentrations (~0.6 to 10 nmol $liter^{-1}$) persisted in the photic layer (~0-100 m) (Fig. 1E). The repeated turbulence profiles (Fig. S2) revealed an order of magnitude higher vertical diffusivity above the volcano (Kz = 3.7±1.9x10^{-5} m^2 s^{-1} at ~50 m, corresponding to the base of the surface mixed layer) compared to the distal open-sea reference site (Kz = 5.2±9.6x10^{-6} m^2 s^{-1}) (Table 1). Combining the measured Kz with the DFe gradients (Table 1 and Supplementary materials), the diffusive DFe vertical supply to the mixed layer above the volcano reached 1.1±1.7x10^{-4} mmol Fe m^{-2} d^{-1}. This is orders of magnitude larger than at the reference site (Table 1), suggesting that Fe-rich fluids released close to the shallow volcano represent a significant Fe source to surface waters. A phosphate supply of 5.4±2.4x10^{-3} mmol m^{-2} d^{-1} accompanied this vertical DFe supply. However, no nitrate supply could be quantified (Table S2).

Along the west to east transect, total chlorophyll-a (Chl*a)* and particulate organic nitrogen stocks peaked in the naturally Fe-fertilized waters at Volcano #1 (Fig. 2). Both were also elevated up and downstream of the source (Fig. 2C, D) consistent with ocean color images (Fig. 2A). This biomass peak was associated with 2 to 8-fold enhanced N_2 fixation rates relative to surrounding waters adjacent to the Arc (p<0.05, Mann-Whitney test) (Fig 2E). The extremely high N_2 fixation rates of >2000 µmol N m^{-2} d^{-1} were associated with ~90-fold higher *Trichodesmium* spp. abundances (~6 x 10^7 *nifH* copies L^{-1}) compared to abundances observed on either side of the Arc (p<0.05, Mann-Whitney test) (Fig. 2F) and a marked phosphate drawdown (~50 nM) in the photic layer. Diazotrophs were favored by the extremely low nitrate concentrations along the transect (Fig. S5).

The particulate organic carbon (POC) export flux was measured using surface tethered sediment traps deployed for 4 days near Volcano #1 and at the reference site. Consistent with model simulations in this region[12], POC export at 170 m and 270 m was 2 to 3 times higher in the Fe-fertilized patch than at the reference site (Table 1), resulting in an excess of POC export of 1.4 to 2.5 mmol C m^{-2} d^{-1} in the fertilized waters. Comparing measurements of water column nitrate+nitrite $\delta^{15}N$ with the $\delta^{15}N$ of sinking particulate N (-0.4± 3.5‰ at 170 m and -0.2± 1.9‰ at 270 m, respectively), the N isotope budget (N_2 fixation end member = -1‰, subsurface nitrate+nitrite $\delta^{15}N$ end member range = 1.3 to 2.2‰) revealed that N_2 fixation supported 77 to 84±154% at 170 m and 66 to 76±83% at 270 m of the export production in the Fe-fertilized area. Collectively, these results suggest that the hydrothermally-driven Fe fertilization fuels planktonic diazotrophs, resulting in enhanced POC export and low $\delta^{15}N$ sinking particulate N compared to subtropical systems not impacted by hydrothermal activity[13].

To confirm the causal link between hydrothermal inputs and diazotroph activity, we conducted novel experiments where hydrothermally-enriched waters collected close to the Volcano #1 caldera were supplied to surface biological communities using 300-L trace metal clean reactors (Fig. 3A, Methods). Increasing fluid additions were added to surface seawater from outside of the direct volcanic influence (21°41.032'S, 174°42.554'W) resulting in consistent increases of DFe concentrations and decreasing pH in the experimental reactors (Fig. S6). Fluid additions enhanced N_2 fixation rates by a factor of 7 to 8 on average over all sampling days compared to those measured in the unamended control (p<0.05, Mann-Whitney test) (Fig. 3B), reaching levels in the same range as *in situ* rates measured above the volcano (Fig. 2E). Likewise, as

observed *in-situ*, *Trichodesmium* abundances increased by a factor of 3 to 5-fold ($p<0.05$, Mann-Whitney test) in fluid-amended reactors (Fig. 3C). Both N_2 fixation rates and *Trichodesmium* abundances decreased at the end of the experiment, likely as a consequence of phosphate depletion in the reactors (Fig. S6), but generally remained higher in the amended reactors compared to those measured in the control.

The Fe supply from the Tonga Arc thus drives in large part upper ocean phenology of biological activity. We estimate that the region of elevated Chl*a* extends ~800 km in longitude and ~450 km in latitude, forming a hot spot of biological activity of ~360,000 km^2 in the middle of the otherwise desert-like WTSP. The trajectories of SVP drifters deployed above Volcano #1 indicate that over a 6-month period, Fe-fertilized water masses can be dispersed regionally and support such an extended Chl*a* patch (Fig. S7). The trajectories provide a bulk representation of complex dynamical processes occurring at smaller scales, involving the South Equatorial current and modulated by mesoscale activity[6, 14], or lateral stirring by filaments[15]. In addition, multiple active vent fields have been (recently) identified along the Tonga Arc and the Lau Basin[9, 11, 16], either at shallow depths (<500 m) or deeper (500-1000 m). Although all active shallow vents have not yet been discovered, with a density estimation of one active volcano center per 12 km of Arc, fertilization processes such as those evidenced at Volcano #1 likely occur at many locations along the Arc, further explaining the regional extent of the Chl*a* patch observed by satellite (Fig. 2A). Finally, we cannot exclude that the few emerged Tonga islands could provide additional nutrients, likely further increasing the intensity of the bloom[17]. Looking more deeply into the 20-year monthly Chl*a* time series (Fig. 2B, S8), we find that, despite interannual variability, the bloom develops every year for at least 6 months in austral summer. This seasonal characteristic is probably linked to the thermal fitness of *Trichodesmium*, who only bloom at temperatures >25°C - reached in the WTSP between November and April (austral summer). To properly account for the seasonal variability of export, we deployed a moored sediment trap at 1000 m for a full annual cycle in the fertilized patch. We show that POC export was 5 times higher in austral summer compared to winter (Fig. S9), resulting in a seasonally-integrated (6 summer months) POC export of 74 mmol C m^{-2}, i.e. 80% of the annual POC export flux.

Compared to shelf-driven natural Fe fertilizations occurring in HNLC (High Nutrient, Low Chlorophyll) waters of the Southern Ocean (SO), the TONGA bloom is generally longer and larger, despite its lower intensity (depth integrated Chl*a*) (Table 1)[18-21]. The total DFe flux (130 nmol Fe m^{-2} d^{-1}) was generally lower than that measured in Fe-enriched waters downstream of the Kerguelen plateau (KEOPS cruise in 2005, 222 nmol Fe m^{-2} d^{-1}[22]) and downstream of the Crozet plateau (CROZEX cruise in 2004, 550 nmol Fe m^{-2} d^{-1}[20]) (Table 1). However, unlike HNLC regions, surface waters of the WTSP are nitrate-depleted, and only N_2-fixing organisms can exploit this new Fe to build biomass and drive carbon export to the deep ocean, as long as sufficient phosphorus remains available. Based on the excess POC export and the excess of DFe supply at the time of the cruise (Table 1), we calculated a fertilization efficiency (defined as the ratio of the POC export to the amount of DFe supplied) of 13200 and 23600 mol C mol^{-1} Fe (at 170 and 270 m, respectively). Although comparisons between studies need to be considered with caution given the different methods used and timescales considered to estimate both excess Fe supply and POC export, this value is somewhat higher than those from artificial mesoscale Fe-addition experiments (e.g. 4300 mol mol^{-1} for SOFeX[23]; 1200 mol mol^{-1} for SERIES[24]), and slightly higher (8600 mol mol^{-1} for CROZEX[20]) or lower (154,000 mol mol^{-1} during KEOPS[22]) than those measured in naturally-fertilized HNLC regions.

Our conceptual view of the ocean Fe cycle has greatly evolved over the past 10 years, highlighting the importance of hydrothermal activity on the Fe cycle[25]. Yet, model simulations suggest that, although hydrothermal inputs associated with mid-ocean ridges (>2000 m) contribute to a significant part of the water column Fe inventory (23% of the ocean), they only directly support 3% of carbon export at 100 m[26]. This is mostly because a large part of that Fe remains in the deep ocean over long time scales[25] and needs to be entrained in surface waters before potentially impacting photosynthetic communities[18, 21]. However, hydrothermal venting also occurs at shallower depths (<500 m) on island arc systems such as the Tonga Arc. Even if scavenging likely removes part of this newly-emitted Fe from the dissolved pool, such shallow sources can supply Fe much more rapidly to surface photosynthetic communities compared to Fe emitted from deeper mid-ocean ridges. The implications of such shallow hydrothermal Fe fertilization in the oligotrophic ocean are highly significant as they fuel surface diazotrophs and export of organic matter to the deep ocean, representing regional hotspot sinks of atmospheric CO_2. We demonstrate here that shallow hydrothermal sources also represent a triggering factor on diazotroph blooms in regions where atmospheric supply of DFe is virtually absent. Such forcing is of the utmost importance to study as climate models predict an expansion of the oligotrophic gyres (40% of our oceans)[27] where diazotrophs will likely thrive. Beyond the oligotrophic oceans, shallow hydrothermal fertilizations are likely to be common in the global ocean, due to the high number of shallow hydrothermal vents associated with island arc systems and submarine volcanic calderas[28] whose exact number/locations are still yet to be discovered[9]. Such systems are also present at higher latitudes, notably in the HNLC waters in the subarctic Pacific and the SO[28]. An evaluation of their impact in these severely Fe-limited systems where surface mixed layers reach the intermediate or even the deep ocean/ water masses is clearly needed.

References

1. N. Gruber, in *Nitrogen in the marine environment*. (2008), pp. 1-50.
2. J. P. Zehr, D. G. Capone, Changing perspectives in marine nitrogen fixation. *Science* **368**, (2020).
3. J. A. Sohm, E. A. Webb, D. G. Capone, Emerging patterns of marine nitrogen fixation. *Nature Reviews Microbiology* **9**, 499-508 (2011).
4. S. Bonnet, M. Caffin, H. Berthelot, T. Moutin, Hot spot of N2 fixation in the western tropical South Pacific pleads for a spatial decoupling between N2 fixation and denitrification. *Proceedings of the National Academy of Sciences* **114**, E2800-E2801 (2017).
5. C. Schlosser *et al.*, Seasonal ITCZ migration dynamically controls the location of the (sub)tropical Atlantic biogeochemical divide. *Proceedings of the National Academy of Sciences of the United States of America* **111**, 1438-1442 (2014).
6. C. Guieu *et al.*, Iron from a submarine source impacts the productive layer of the Western Tropical South Pacific (WTSP). *Scientific Reports* **8**, 9075 (2018).
7. L. Bopp *et al.*, Diazotrophy as a key driver of the response of marine net primary productivity to climate change. *Biogeosciences Discussions*, (2021).
8. C. E. J. de Ronde *et al.*, in *Volcanic, Geothermal, and Ore-Forming Fluids: Rulers and Witnesses of Processes within the Earth*. (Society of Economic Geologists, 2005), vol. 10, pp. 0.
9. C. R. German *et al.*, Hydrothermal impacts on trace element and isotope ocean biogeochemistry. *Phil. Trans. R. Soc. A* **374**, 20160035 (2016).

10. J. E. Lupton, D. G. Pyle, W. J. Jenkins, R. Greene, L. Evans, Evidence for an extensive hydrothermal plume in the Tonga-Fiji region of the South Pacific. *Geochem Geophy Geosy* **5**, (2004).
11. G. Massoth *et al.*, Multiple hydrothermal sources along the south Tonga arc and Valu Fa Ridge. *Geochemistry, Geophysics, Geosystems* **8**, (2007).
12. J. A. Resing *et al.*, Basin-scale transport of hydrothermal dissolved metals across the South Pacific Ocean. *Nature* **523**, 200-203 (2015).
13. A. N. Knapp *et al.*, Distribution and rates of nitrogen fixation in the western tropical South Pacific Ocean constrained by nitrogen isotope budgets. *Biogeosciences* **15**, 2619-2628 (2018).
14. L. Rousselet *et al.*, Large- to submesoscale surface circulation and its implications on biogeochemical/biological horizontal distributions during the OUTPACE cruise (southwest Pacific). *Biogeosciences* **15**, 2411-2431 (2018).
15. A. de Verneil, L. Rousselet, A. M. Doglioli, A. A. Petrenko, T. Moutin, The fate of a southwest Pacific bloom: gauging the impact of submesoscale vs. mesoscale circulation on biological gradients in the subtropics. *Biogeosciences* **14**, 3471-3486 (2017).
16. S. E. Beaulieu, E. T. Baker, C. R. German, A. Maffei, An authoritative global database for active submarine hydrothermal vent fields. *Geochem Geophy Geosy* **14**, 4892-4905 (2013).
17. M. Messie *et al.*, The Delayed Island Mass Effect: How Islands can Remotely Trigger Blooms in the Oligotrophic Ocean. *Geophysical Research Letters* **47**, (2020).
18. M. Ardyna *et al.*, Hydrothermal vents trigger massive phytoplankton blooms in the Southern Ocean. *Nat Commun* **10**, 2451 (2019).
19. S. Blain, S. Bonnet, C. Guieu, Dissolved iron distribution in the tropical and sub tropical South Eastern Pacific. *Biogeosciences* **5**, 269–280 (2008).
20. R. T. Pollard *et al.*, Southern Ocean deep-water carbon export enhanced by natural iron fertilization. *Nature* **457**, 577-580 (2009).
21. C. M. S. Schine *et al.*, Massive Southern Ocean phytoplankton bloom fed by iron of possible hydrothermal origin. *Nat Commun* **12**, 1211 (2021).
22. S. Blain *et al.*, Effect of natural iron fertilization on carbon sequestration in the Southern Ocean. *Nature* **446**, 1070-1074 (2007).
23. K. O. Buesseler, J. E. Andrews, S. M. Pike, M. A. Charette, The effect of iron fertilization on carbon sequestration in the Southern ocean. *Science* **304**, 414-417 (2004).
24. P. W. Boyd *et al.*, The decline and fate of an iron-induced subarctic phytoplankton bloom. *Nature* **428**, 549-553 (2004).
25. A. Tagliabue *et al.*, The integral role of iron in ocean biogeochemistry. *Nature* **543**, 51-59 (2017).
26. A. Tagliabue, O. Aumont, L. Bopp, The impact of different external sources of iron on the global carbon cycle. *Geophysical Research Letters* **41**, 920-926 (2014).
27. J. J. Polovina, E. A. Howell, M. Abecassis, Ocean's least productive waters are expanding. *Geophysical Research Letters* **35**, (2008).
28. J. A. Hawkes, D. P. Connelly, M. J. A. Rijkenberg, E. P. Achterberg, The importance of shallow hydrothermal island arc systems in ocean biogeochemistry. *Journal of Geophysical Research*, (2014).

Acknowledgments: The dataset presented here resulted from the efforts of many individuals both onboard and on land who contributed to the success of the expedition. We thank the captain and the crew of the R/V *L'Atalante* (TGIR Flotte, operated by IFREMER), in particular S. Laville Saint-Martin and J. Le Doare for their help during the multibeam survey, as well as the Technical Division INSU for the provision of the equipment. We thank Mr Lucas Jr for the English editing. Finally we are very grateful and thank JP Gattuso, S. Blain, A. Tagliabue and L. Guidi for their advice on the manuscript.

Funding:
Agence Nationale de Recherche grant ANR-18-CE01-0016 (SB, CG)
A-Midex grant TONGA (SB, CG)
Institut National des Sciences de l'Univers Les Enveloppes Fluides et l'Environnement grant TONGA (SB, CG)
TGIR Flotte océanographique française TONGA cruise (CG, SB)
MEMESTRA Grant (CB)
US NSF-OCE 1829797 (ANK)

Author contributions:
Conceptualization: SB, CG
Methodology: SB, CG, CB, FG
Investigation: SB, CG, VT, CB, FG, MB, DGS, JMG, OG, JH, CL, EP, GS, CT
Data curation: SB, CG, VT, CB, PBA, FG, MB, ANK, YC, DGS, HJF, JH, NL, SN, ALR, GS
Visualization: SB, CG, CB, FG, PBA, ANK, HJF
Writing – original draft: SB, CG
Writing – review & editing: All
Competing interests: Authors declare that they have no competing interests.

Data and materials availability: All data are available in the main text or the supplementary materials. The delta ^{15}N data are deposited to the BCO-DMO database https://www.bco-dmo.org/dataset/869963.

Supplementary Materials
Materials and Methods
Figs. S1 to S9
Tables S1 to S2
References (1-28)

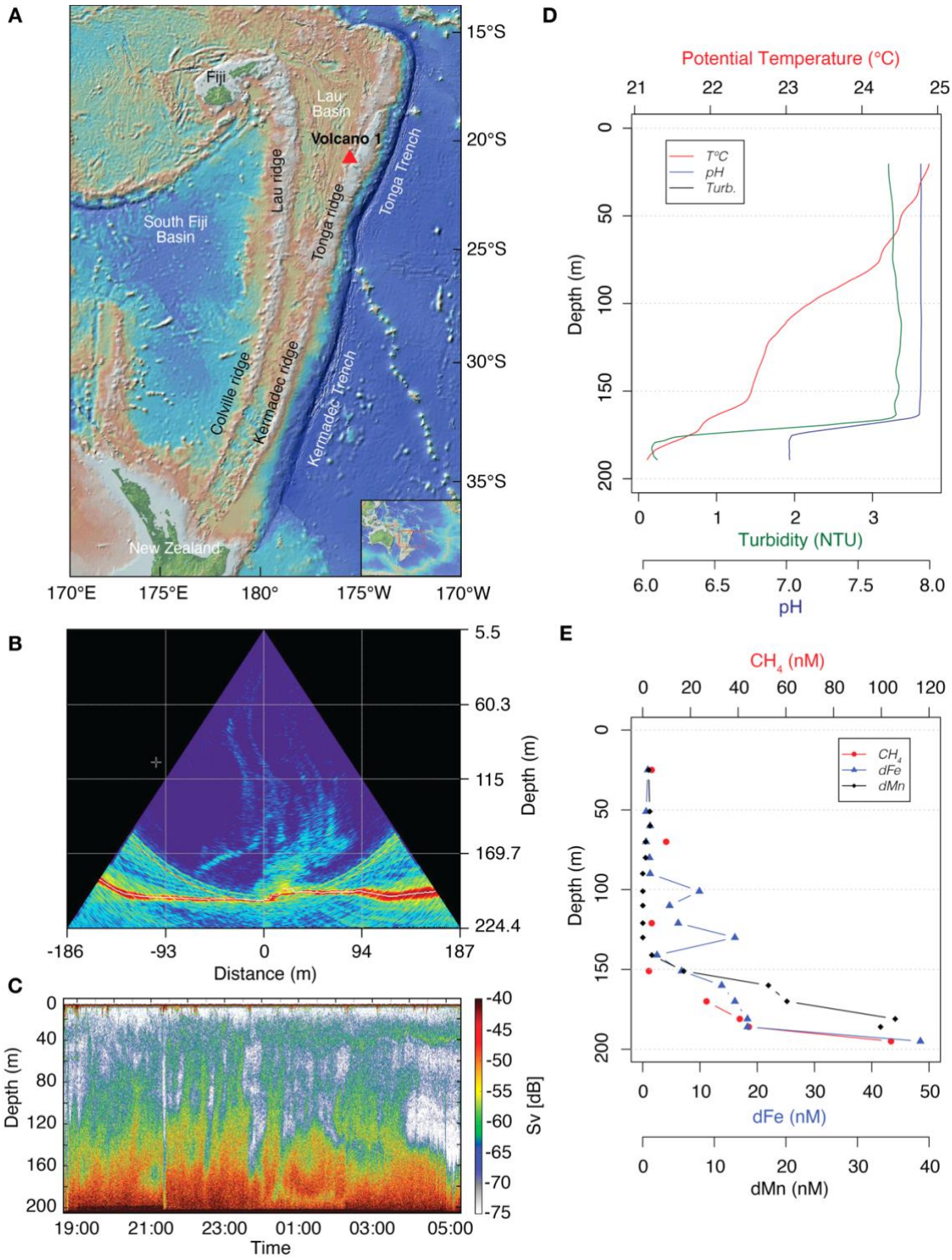

Fig. 1. Acoustic, optical and chemical anomalies measured above Volcano #1. (A) Location map showing the Tonga volcanic arc system and Volcano #1 (V1, red triangle, 21.165°S; 175.164°E). (B) Multibeam echo sounder image (EM710, 70-110 kHz) showing hydrothermal gas and fluid emissions from the seafloor rising up to ~30 m below the surface. (C) Time series (11h) of acoustic signal detected by the sounder EK60 (38kHz) showing a 'bubble bath' above Volcano #1 (visualization threshold -75dB). (D) Vertical CTD profiles of temperature, pH, turbidity, and Eh in the main acoustic signal. (E) Vertical profiles of methane (CH_4, nM), dissolved Mn (nM), and dissolved Fe (nM) concentrations above Volcano #1.

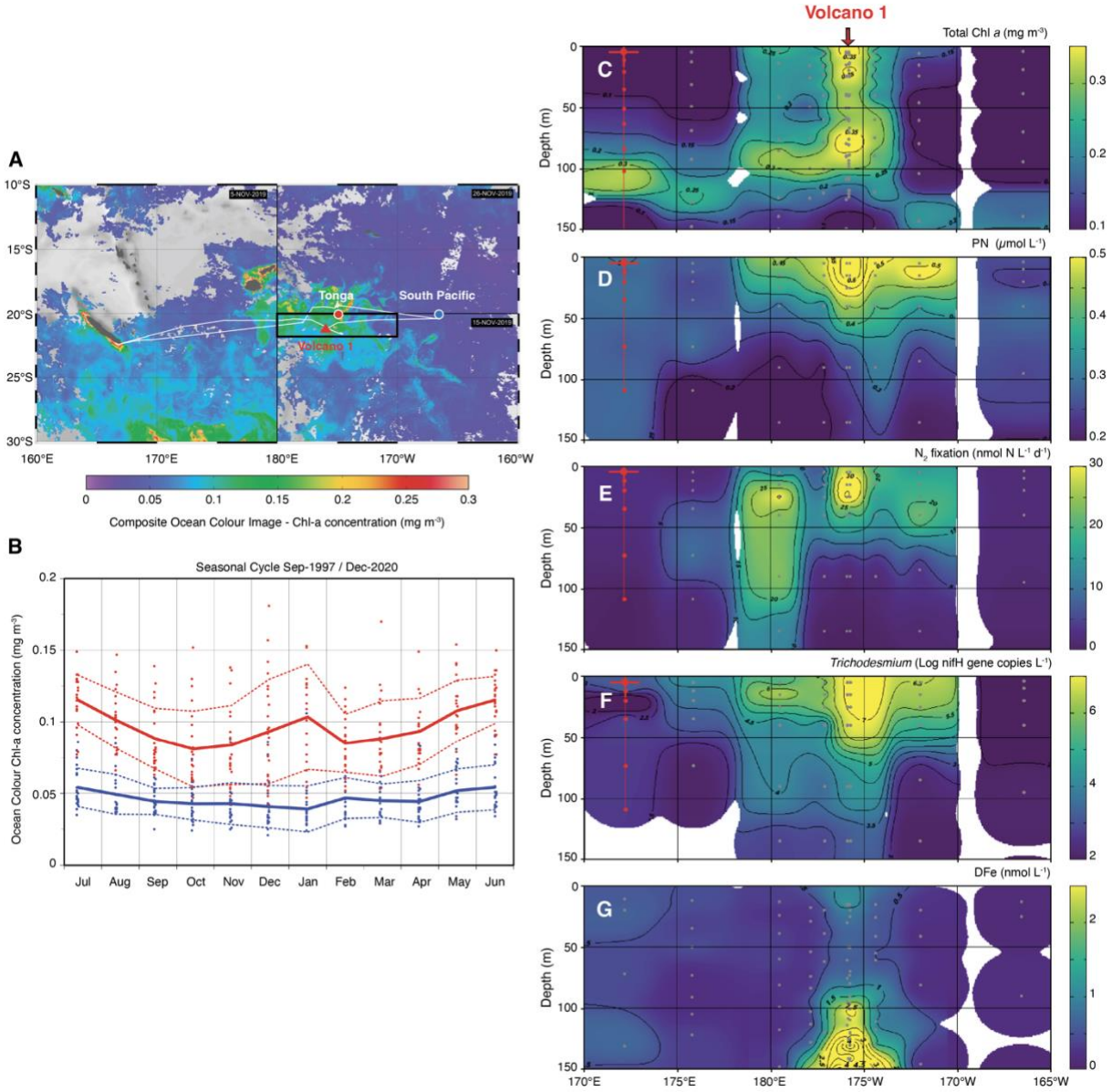

Fig. 2. West to east transect showing the Chlorophyll patch in the vicinity of Tonga and associated biogeochemical and biological parameters. (A) Surface Chlorophyll MODIS composite averaged over the time period corresponding to the TONGA cruise (1 November-6 December 2019) at a resolution of 4 km. (B) Monthly climatology of [Chlorophyll] from a 23 years-time series (GLOBCOLOR product) at 20°S, 175°W (Tonga arc, red dot on the map) and a reference site in the South Pacific Gyre (blue dot). Horizontal and vertical distributions of (C) Total Chl*a* concentrations (µg L^{-1}), (C) Particulate organic nitrogen concentrations (µmol L^{-1}), (D) N_2 fixation rates (nmol N L^{-1} d^{-1}), (E) *Trichodesmium* abundances (Log nifH gene copies L^{-1}), (F) Dissolved Fe concentrations (nmol $liter^{-1}$). Y axis: pressure (dbar), X axis: longitude; grey dots correspond to sampling depths at the various stations.

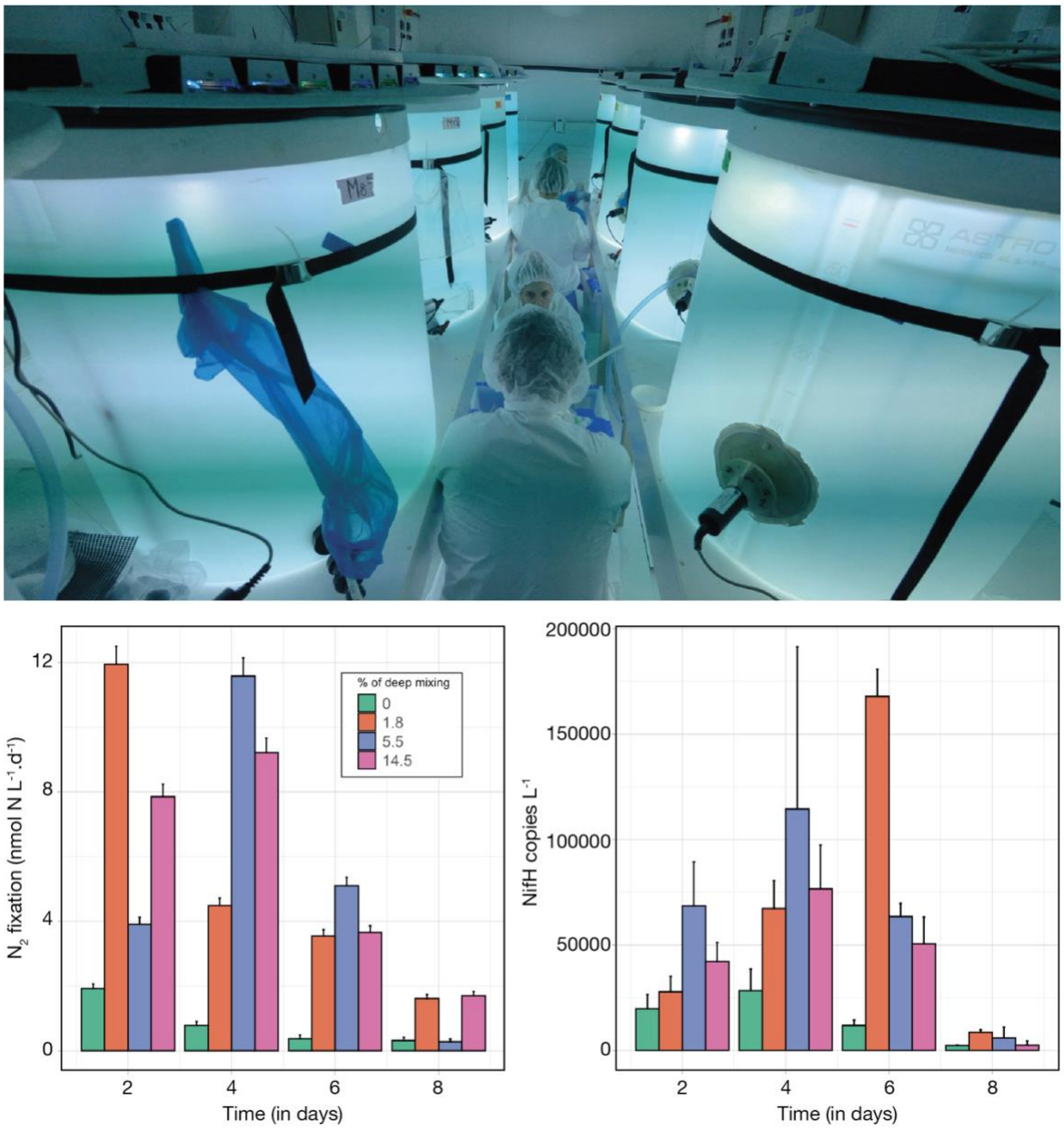

Fig. 3. Experimental evidence of the impact of hydrothermally-enriched water additions on diazotroph communities. (A) Picture showing the experimental 300-L reactors inside the trace metal clean van onboard. Temporal evolution of (B) N_2 fixation rates (nmol N L^{-1} d^{-1}), (C) *Trichodesmium* abundances (*nifH* gene copies L^{-1}) along the 196h of the experiment in the control treatment (no fluid addition), and in the reactors amended with 1.8%, 5.5%, and 14.5% of hydrothermal fluids collected near the caldera of Volcano #1 (~200 m depth). Error bars correspond to standard deviations on triplicate analyses.

Table 1. Carbon and Fe budgets in the naturally-fertilized region of the Tonga volcanic Arc and the distal reference site, and comparisons with natural fertilizations in HNLC regions.

	TONGA		CROZEX (2,5)	KEOPS (2,3)
	+Fe (Volcano #1)	-Fe (Gyre)		
Bloom area (km^2)	360000	No bloom	90000	45000
Bloom duration (d)	180	-	58	75-105
Integrated Chla over the euphotic zone (mg Chl*a* m^{-2})	39	-	98.1	72-318
Vertical diffusivity (Kz, $m^2 s^{-1}$)	$3.7 \pm 1.9 \times 10^{-5}$	$5.2 \pm 9.6 \times 10^{-6}$		
Vertical DFe gradient (mol m^{-4})	$3.1 \pm 4.7 \times 10^{-8}$	$7.8 \pm 3.1 \times 10^{-11}$		
Vertical DFe diffusive flux (mmol m^{-2} d^{-1})	$1.1 \pm 1.7 \times 10^{-4}$	$3.5 \pm 3.1 \times 10^{-8}$	6.0×10^{-5}	3.1×10^{-5}
Atmospheric DFe supply (mmol m^{-2} d^{-1}) (1)	2.0×10^{-5}	2.5×10^{-5}	1.0×10^{-4}	1.7×10^{-6}
Horizontal DFe supply (mmol m^{-2} d^{-1})	0 (4)	0 (4)	3.9×10^{-4}	1.9×10^{-4}
Total DFe supply (mmol m^{-2} d^{-1})	1.3×10^{-4}	2.5×10^{-5}	5.5×10^{-4}	2.2×10^{-4}
Total annual DFe supply (mmol m^{-2})	2.3×10^{-2}	-	3.2×10^{-2}	2.0×10^{-2}
POC export 170 m (mmol C m^{-2} d^{-1})	3.1	1.7		
POC export 270 m (mmol C m^{-2} d^{-1})	3.9	1.4		
"Excess" C sequestration efficiency Ceffx 170 m (mol C mol^{-1} Fe)	13200	-	8640	154000
"Excess" C sequestration efficiency Ceffx 270 m (mol C mol^{-1} Fe)	23600	-		

(1) Guieu et al., (2018)
(2) Morris & Charrette, (2013)
(3) Blain et al., (2007) updated by Chever et al., (2010)
(4) The main flux is from below, lateral advection is likely negligible
(5) Pollard et al., (2009)

Science
AAAS

Supplementary Materials for

Natural iron fertilization by shallow hydrothermal sources fuels diazotroph blooms in the Ocean

Authors: Sophie Bonnet[1], Cécile Guieu[2], Vincent Taillandier[2], Cédric Boulart[3], Pascale Bouruet-Aubertot[4], Frédéric Gazeau[2], Matthieu Bressac[2], Angela N. Knapp[5], Yannis Cuypers[4], David González-Santana[6,7], Heather J. Forrer[5], Jean-Michel Grisoni[2], Olivier Grosso[1], Jérémie Habasque[6], Mercedes Jardin-Camps[1], Nathalie Leblond[2], Frédéric Le Moigne[1], Anne Lebourges-Dhaussy[6], Caroline Lory[1], Sandra Nunige[1], Elvira Pulido-Villena[1], Andrea L. Rizzo[9,10], Géraldine Sarthou[6], Chloé Tilliette[2]

***Correspondence to:** sophie.bonnet@mio.osupytheas.fr, cecile.guieu@imev-mer.fr

This PDF file includes
Materials and Methods
Figs. S1 to S9
Tables S1 to S2
References (1-29)

Materials and Methods

Fieldwork design

Data were acquired during the GEOTRACES-endorsed TONGA (Shallow hydroThermal sOurces of trace elemeNts: potential impacts on biological productivity and the bioloGicAl carbon pump) expedition (October 30-December 6, 2019, https://doi.org/10.17600/18000884) on board the R/V L'Atalante). The general strategy consisted in: i) a 3000 km transect crossing the Tonga volcanic arc at 20-21°S, sampling 12 stations located both sides of the arc, namely Melanesian archipelago waters and South Pacific Gyre waters, ii) an intensive 5-days survey on the Tonga volcanic arc to locate a 'case study' shallow (~200 m) volcano associated with hydrothermal activity (Volcano #1), to investigate the direct potential effect of hydrothermal fluids on biological stocks and fluxes.

Acoustic plume detection

Shipborne single and multibeam echosounder surveys were carried out over the targeted volcano. Surveys were performed at <7 knots using the hull-mounted EM-122 and EM-710 echosounders of R/V L'Atalante, operating at a frequency of 12 kHz (for depths >1000m), and 70 to 100 kHz (for lower depths), respectively. Our strategy allowed us to establish a high-resolution (10 m) bathymetric mapping of the targeted area; simultaneously, acoustic anomalies directly identified on the screen during the survey and corresponding to putative fluid emissions were reported in order to get all the coordinates where anomalies were detected. Acoustic anomalies were considered as attributable to hydrothermal emissions if they were connected to the seafloor and reproducible over time. After having located the site showing the highest anomaly (Fig. 1A), the second step consisted in deploying a conductivity–temperature–pressure (CTD) rosette fitted with Niskin bottles and additional physical and chemical sensors (see next paragraph) to confirm the presence of chemical and physical/optical anomalies related to hydrothermal plumes in the water column. The R/V remained 11 hours above and within a short distance from that source, also allowing to perform a time-series of acoustic anomalies using a calibrated[1] Simrad EK60 echosounder operating at 38 kHz with an average ping interval of 5 s (Fig. 1 C). The pulse length was set at 1024 µs and transmit powers was 2000 W. The water column was sampled down to 800 m depth.

Optical and chemical plume detection

The chemical plume survey was carried out using a 12-Niskin CTD-rosette frame fitted with two turbidimeters (Seapoint Turbidity Meters), a pH sensor and a Eh sensor (both from AMT GmBH), interfaced to a SBE911+ (Seabird Electronics). The CTD-rosette was deployed either as vertical casts or as towed casts ('tow-yo casts'). During vertical casts, the CTD-rosette was lowered in the water column at 1 m per second or less to the deepest point. Niskin bottles were fired during up-casts at different levels in the water column, whenever an anomaly of T, S, turbidity or Eh appeared on the real-time data display. The tow-yo casts consisted in lowering and raising the CTD-rosette between a constant set depth and a few meters above the seafloor while the ship moved along a transect at a maximum speed of 0.4 knot.

Water samples for dissolved gas analysis (methane (CH_4), Helium (He)) were drawn from the Niskin bottles and processed straight after the CTD-rosette was brought back on board. 20 mL-headspace glass vials were flushed with the water from the Niskin bottles, filled until overflow, poisoned, and crimp-sealed to avoid any air contamination. Water samples for Helium isotopes analysis were transferred from the Niskin into copper tubes that were clamped on both ends paying attention to avoid the entrapment of any air bubbles. This storage is typical of water sampling aimed at measurements of dissolved noble gases[2].

Dissolved CH_4 concentrations were determined on board using the headspace extraction technique followed by GC-FID. Duplicates were analyzed back on shore on a Shimadzu GC-BID coupled to a HS-20 to confirm the on-board measurements. He isotopes were analyzed in the noble gas laboratory of INGV-Palermo (Italy). Copper tubes were connected to a stainless steel extraction line maintained under high-vacuum and equipped with a pyrex bulbe and a manometer. The extraction of helium and neon dissolved in the water was carried out by following standard protocols[2, 3]. The following He (^{3}He, ^{4}He) and ^{20}Ne isotopic measurements followed the analytical method reported in Rizzo et al., (2016)[4]. The concentrations of He and Ne are reported in cc/l STP, while the ^{3}He/^{4}He ratio is expressed as R/Ra (being Ra the He isotopic ratio of air and equal to 1.39×10^{-6}).

Dissolved Fe and Mn concentrations

Seawater samples were collected above Volcano #1 and at 12 stations along the transect according to the GEOTRACES guidelines (www.geotraces.org/images/Cookbook.pdf), using a Trace Metal Clean Rosette (TMR, General Oceanics Inc. Model 1018 Intelligent Rosette) attached to a 6 mm Kevlar line and fitted with 24 Go-Flo bottles. Immediately after collection, the entire rosette was transferred into a clean container for sampling. The cleaning protocols for sampling bottles and equipment also followed the GEOTRACES Cookbook. Samples for the determination of total dissolved iron (DFe) and manganese (DMn) concentrations were filtered on-line through 0.45 µm using a polyethersulfone filter (Supor®). All samples were acidified within 24h of collection with ultrapure hydrochloric acid (HCl, Merck, 0.2%, final pH 1.7). Dissolved iron (DFe) were analyzed by Flow Injection Analysis with chemiluminescence detection[5]. Dissolved Mn was analyzed using a preconcentration system SeaFAST coupled to a high resolution magnetic sector field inductively coupled mass spectrometer (HR-ICP-MS, Element XR) method following Tonnard et al. (2020)[6].

Vertical eddy diffusivity (Kz) measurements and DFe vertical fluxes estimates

Microstructure measurements were performed using a vertical microstructure profiler 'VMP250' (Rockland Scientific). This tethered profiler was equipped with microstructure sensors, two shear sensors, and two temperature sensors, as well as with Sea-Bird temperature and conductivity sensors.

Four VMP profiles were performed above Volcano #1. The dissipation rate of turbulent kinetic energy (epsilon) was inferred from centimeter-scale shear measurements as described in Bouruet-Aubertot et al, (2018)[7]. The vertical eddy diffusivity (Kz) was then inferred from the kinetic energy dissipation rate using the Osborn (1980)[8] relationship:

$$Kz = Gamma \times epsilon \, N^{-2}$$

where Gamma is a mixing efficiency defined as the ratio between the buoyancy flux and the dissipation rate, and N the buoyancy frequency. The kinetic energy dissipation rate is computed over 1m bin, and a 8-m moving average is then applied, while the buoyancy frequency square is inferred from the VMP Sea-Bird temperature and conductivity sensors, with a 8-m moving average applied on this signal after preliminary processing to eliminate spurious spikes on the salinity signal. Gamma is set to 0.2 provided that turbulence intensity values fall within the intermediate regime where the Osborn relationship applies (see further details in Bouruet-Aubertot et al, 2018)[7].

DFe vertical supply at station Volcano #1 was estimated based on turbulent diffusive flux:

$$F = -Kz \times dcFe/dz$$

where dcFe/dz is the vertical gradient of DFe concentration, cFe. As the DFe concentration profile displays variations, the DFe turbulent diffusive flux is either upward or downward with strong variations in absolute value as a result of vertical eddy diffusivity variations within 1 or 2 orders of magnitude (Fig. S2). Mean values of DFe input as well as their standard deviations were computed over the the mixed layer (within [40m-60m]), where most of the biological biomass needing Fe was concentrated.

The instrument was lost after Volcano #1, and in the absence of VMP measurements at the reference site, the vertical eddy diffusivity, Kz, was inferred from CTD measurements. This Kz estimate was based on the Thorpe scale method[9, 10] when density overturns are detected by CTD with a given threshold for noise taken here to 3x10-4 kg.m-3. Kz (term 1) is proportional to the mean square of vertical displacements within the overturn. In addition, a 'background' value for Kz (term 2) was inferred from the strain computed over vertical segments of 256 m extension, following Kunze et al (2006)[11]. The intermediate Kz value equals the sum (1) + (2).

The method was validated at the Volcano#1 station where CTD data were collected just after the VMP profiles (TMC12). The 'background' value for Kz (term 2) was computed over the length of the CTD profile, 194 m, the proportionality constant for Kz term 1 was adjusted with VMP measurements and a 20 m moving average was applied to Kz term1 (see Fig. S3).

The same procedure was applied at the reference station for the computation of Kz as described above. An optimal interpolation was applied to DFe values in the first 1000 m in order to eliminate unrealistic variations, of the order of 10^{-7} mol m^{-3} prior to the flux computation (Fig. S4). Vertical eddy diffusivity, vertical gradient of DFe concentration and turbulent diffusive flux within the base of the mixed layer and the ferricline are displayed in Table 1.

SVP drifters trajectories

Three clusters, each composed of 5 SVP drifters have been deployed at the Volcano #1 station and at two additional stations along the Tonga arc (Station 12: 20°43S; 177°52W and Station 10: 19°25,16S; 174°54.7). Drifters are composed of a 35 cm surface floats and a holey sock drogues centered at 15 m depth. GPS-based tracking is sent by Iridium communication. The obtained trajectories have a temporal resolution of some hours up to one day. Raw data are presented in Fig. S7. Patterns of dispersion appear contrasted for the three sites: in the western edge of the Lau Basin (left panel), trajectories indicate westward advection during the first three months. On the other hand, in the eastern site of the Lau Basin (middle and right panels), advective components are reduced and relative dispersion is the predominant pattern. Although qualitative, this description suggests larger horizontal eddy diffusivity along the Tonga arc compared to the Lau Basin.
The Tonga arc might be subject to intense dynamical features that occur in the surface layer, associated to the interaction of a steep topographic sill and basin-scale current system in the sub-tropical band. Drifter trajectories provide a bulk representation of a complex underlying dynamics, which develops at smaller scales with significant vertical component (upwelling).
In consequence for the iron budgets above the Volcano site, transports in the surface layer would be predominantly due to horizontal mixing rather than advection.

Ocean Color

Chlorophyll concentrations (mg m^{-3}) were provided by the global Ocean Color satellite observations from the Copernicus-GlobColour database. Two products have been used for this study, both processed from multi-satellite sensors with a spatial resolution of 4 km, and

reprocessed using a consolidated input dataset and a unique algorithm: the composite image contemporary to the cruise (Fig. 1A) was extracted from the daily "Level 3" product (https://doi.org/10.48670/moi-00098). The five seasonal cycles (Fig. 1B and Fig. S8) were extracted from the "Level 4" product ("cloud free") (https://doi.org/10.48670/moi-00100), in which a temporal averaging method was applied to fill-in missing data values. Each seasonal cycle was computed as follows: 23-year time series (from September 1997 to December 2020) were extracted at five locations along the 20°S parallel. For each month of the year, a mean value and standard deviation were computed.

Nitrate, phosphate concentrations

Nitrate, phosphate concentrations were measured at 12 stations along the west to east transect. Seawater samples were collected at 6 to 9 depths between 0 and 200 m using Niskin® bottles attached to the CTD-rosette. Samples for the quantification of nitrate and phosphate concentrations were collected in acid-washed polyethylene bottles after online filtration (0.2 µm, Sartorius Sartobran P capsule), frozen at -20°C until analysis. Concentrations were determined using standard colorimetric techniques[12] on a Bran Luebbe AA3 autoanalyzer. Quantification limits for the procedures were 0.05 µmol liter^{-1} for nitrate and 0.02 µmol liter^{-1} for phosphate. The same procedures were used for samples collected in the minicosms (see below).

Particulate organic nitrogen concentrations

Particulate organic nitrogen concentrations were measured at 9 stations along the west to east transect. Seawater samples were collected in 4.4 polycarbonate bottles at 6 depths between 0 and 150 m using Go-Flo bottles mounted on the trace metal clean rosette. The entire bottle was filtered onto pre-combusted (450°C, 4h) 25 mm diameter glass fiber filters (GF/F, Whatman, 0.7 µm nominal pore size). Filters were subsequently dried at 60°C for 24 h before analysis of $^{15}N{=}^{14}N$ ratios and particulate N (PN) using an elemental analyzer coupled to a mass spectrometer (EA-IRMS, Integra 2, SerCon Ltd) as described in Bonnet et al. (2018)[13].

N_2 fixation rates

N_2 fixation rates were measured under trace metal clean conditions at 9 stations along the west to east transect. Seawater samples were collected in triplicate 2.3 polycarbonate bottles at 6 depths between 0 and 150 m using Go-Flo bottles mounted on the trace metal clean rosette. Rates were measured using the $^{15}N_2$ assimilation technique; the $^{15}N_2$ bubble technique was intentionally chosen to avoid any potential overestimation due to trace metal and dissolved organic matter contaminations often associated with the preparation of the $^{15}N_2$-enriched seawater[14], as both have been found to control N_2 fixation or *nifH* gene expression in this region[15, 16]. Bottles were amended with 2 mL of 98.9 at.% $^{15}N_2$ (Cambridge isotopes), and incubated in on-deck incubators connected to surface circulating seawater and shaded at the specified irradiances using blue screening. Incubations were stopped by filtering the entire incubation bottle onto pre-combusted (450°C, 4h) 25 mm diameter glass fiber filters (GF/F, Whatman, 0.7 µm nominal pore size). Filters were subsequently dried at 60°C for 24 h before analysis of $^{15}N{=}^{14}N$ ratios and particulate N (PN) determinations using an elemental analyzer coupled to a mass spectrometer (EA-IRMS, Integra 2, SerCon Ltd) as described in Bonnet et al. (2018)[13]. The $^{15}N/^{14}N$ ratio of the N_2 pool available for N_2 fixation (the term AN_2 used in Montoya et al., 1996)[17] was measured in all incubation bottles by membrane inlet mass spectrometry (MIMS)[18] to ensure accurate rate calculations as fully described in Bonnet et al., (2018)[13]. The same procedures were used for samples collected in the minicosms (see below).

Trichodesmium spp. abundances

Trichodesmium spp. abundances were estimated using quantitative PCR (qPCR) targeting the *nifH* gene, which encodes a subunit of the nitrogenase enzyme. Discrete seawater samples (2 L) were collected using the TMC-rosette at the same depth as samples for N_2 fixation, filtered using a peristaltic pump onto 0.2 µm Supor (Cole Parmer, Vernon Hills, IL) filters, frozen in liquid nitrogen, and stored at -80°C until processed. The DNA extraction was conducted using published protocols[19]. The abundance of *Trichodesmium* spp. was determined using TaqMan qPCR assays with primer-probe sets for *Trichodesmium*[20] as fully described in Turk-Kubo et al., (2015)[21]. The same procedures were used for samples collected in the minicosms (see below).

POC export fluxes

A surface tethered drifting mooring line was deployed during the cruise at 10 nm west of Volcano #1 (21°9.55S;175°54.29W) for 4 to 5 days and in a distal site not impacted by hydrothermal sources (reference site, 20°23.37S; 166°25.81W) in the South Pacific Gyre (Fig. 1). The line was equipped with C-RESPIRE particle interceptors/incubators at 2 depths: 170 m and 270 m. C-RESPIRE non-intrusively intercepts settling particles colonized by bacteria, and then subsequently incubates them at in situ temperature and pressure conditions within the same device[22, 23]. After the particle collection phase, C-RESPIRE provides rates of particle remineralization (predominately by particle-attached bacteria) derived from the change in dissolved oxygen concentration measured by an optode. At the end of the deployment, a triplicate set of aliquots was filtered onto 25-mm diameter pre-combusted (4 h at 450°C) glass microfiber filters (Whatman GF/F), which were subsequently dried for 24 h at 60°C, pelleted and from which particulate organic N (PON), δ^{15}N-PON and C (POC) were analyzed by EA-IRMS (Elemental Analyzer-Isotope Ratio Mass Spectrometry) using an Integra 2 (Sercon) mass spectrometer. The obtained residual POC fluxes were corrected for bacterial remineralization using O_2 consumption rates and a C:O_2 conversion factor (117/170[24]) to provide reconstructed POC fluxes.

Another fixed mooring line was also deployed for one year in the fertilized patch (Station 12: 20°42.03S; 177°51.23W). The mooring line was instrumented with a Technicap PPS5 (1 m^2 collecting area, aspect ratio (height/width) of 5.2) sediment trap and inclinometer (NKE S2IP) at a depth of 1000 m (seafloor depth 2000 m). A conductivity–temperature–pressure (CTD) sensor (Sea-Bird SBE 37) and a current meter (Nortek Aquadopp) were placed on the mooring line 35 m beneath the sediment trap. The sediment trap collection period started on 2 December 2019 and continued until 18 October 2020. The sediment trap was composed of 24 rotating sample cups (250 mL) filled with a 5% formalin hypersaline solution buffered with sodium tetraborate at pH 8. Rotation of the carousel was programmed to sample short intervals of 13.9 days. Samples were treated following the standard JGOFS' protocol (as described in Guieu et al., 2005[25]). Total carbon, particulate organic carbon (POC) (after removing inorganic carbon by acidification with HCl 2N), were measured on a CHN elemental analyzer (2400 Series II CHNS/O Elemental Analyzer, Perkin Elmer).

Nitrate+Nitrate isotope analysis

The isotopic analysis of nitrate+nitrite was conducted at Florida State University in the Knapp Laboratory. The δ^{15}N of nitrate+nitrite was determined using the "denitrifier" method[26, 27]. The δ^{15}N of nitrate+nitrite was analyzed using a continuous flow ThermoFisher Delta V Advantage IRMS interfaced with a Gasbench II[26, 28]. International reference materials including IAEA-NO_3 and USGS34 were included in all runs to allow for isotopic calibration.

This analysis was performed on nitrate+nitrite samples with concentrations >1.0 µM. Using this method, we report δ15N nitrate+nitrite values with a SD of <0.2‰.

Mixing experiment with increasing additions of hydrothermally-enriched seawater

Mixing experiments were performed tanks installed in a clean, temperature-controlled container. The tanks were made of high-density polyethylene (HDPE) and were trace-metal-free in order to avoid contaminations, with a height of 1.09 m, a diameter of 0.68 m, a surface area of 0.36 m^2 and a volume of 0.3 m^3 (300 L). Each tank was equipped with a lid containing six rows of LEDs (Alpheus©). Each of these rows were composed of blue, green, cyan and white units in order to mimic the natural sun spectrum. Photosynthetically active radiation (PAR; 400–700 nm) and temperature were continuously monitored in each tank using respectively QSL-2100 Scalar PAR Irradiance Sensors (Biospherical Instruments©) and pt1000 temperature sensors (Metrohm©) connected to a D230 datalogger (Consort©).

On November 11th 2019, five tanks were filled under trace metal clean conditions using a high-speed peristaltic pump (Verder© VF40, flow of 1200 L h^{-1})[29] with surface seawater (~5 m) sampled East of the Tonga arc (21°41.032S, 174°42.554W), outside of the influence of volcanic activity. After homogeneously filling all tanks up to 275 L (performed within 2 h), one tank was immediately sampled and emptied in order to characterize the biogeochemical conditions in the surface water end-member before mixing. Upon arrival at the Volcano #1 station, hydrothermally-enriched seawater was pumped at ~200 m where the maximal acoustic signal was recorded (see main text), using the same protocol as previously described and stored in the tank that had been previously emptied. From this tank, after sampling for the initial characterization of the hydrothermal fluid, precise volumetric additions were performed in each experimental tank following the removal of the corresponding surface water in order to maintain a final volume of 275 L in all tanks. We added increasing amounts of hydrothermally-enriched water: 0% (Control) to 1.8%, 5.5% and 14.5% in volume. Sampling was performed 12h, 24h, 48h, 96h, 144h and 216h after mixing for pH, DFe, nitrate and phosphate concentrations. The biological response of diazotrophs (N_2 fixation rates and *Trichodesmium* abundances) was measured after 48h, 96h, 144h and 196h.

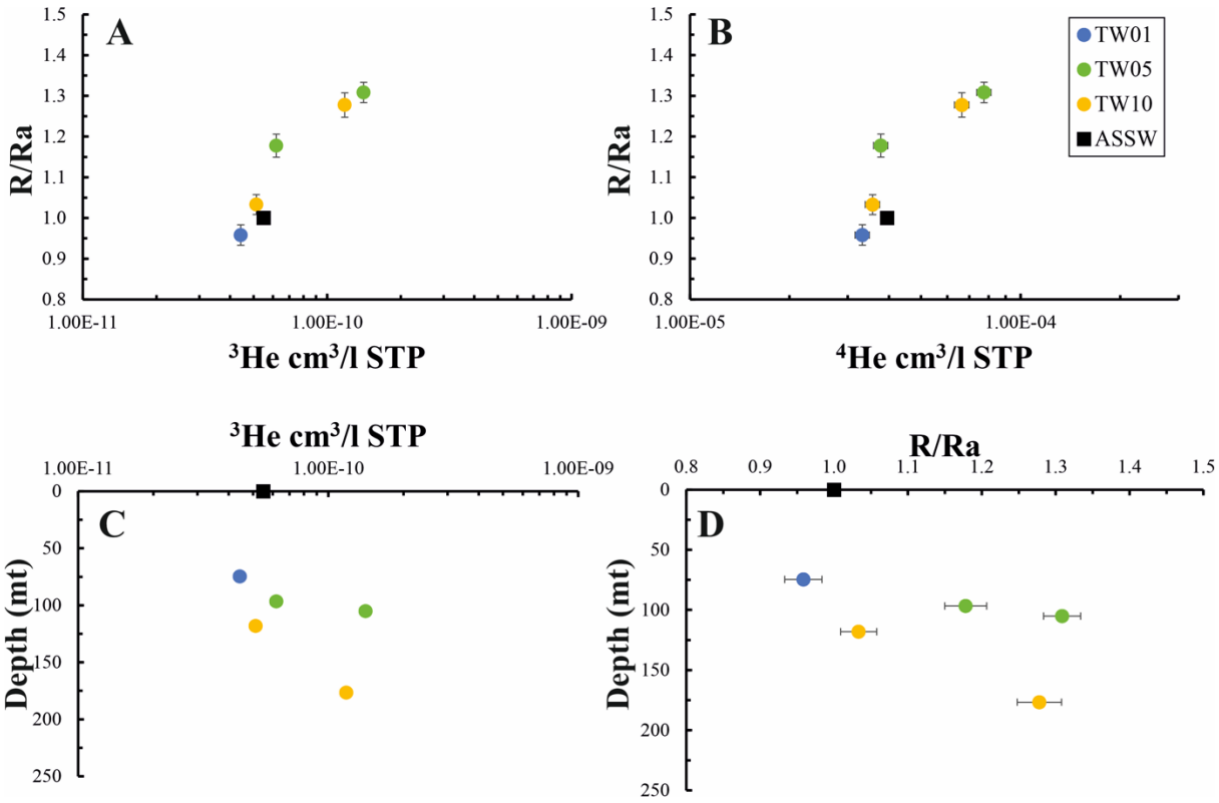

Fig. S1. He analyses above Volcano #1. R/Ra values vs concentrations in cc/l STP (Standard Temperature and Pressure) of ^{3}He (A) and ^{4}He (B) in water samples from three distinct vertical profiles performed above Volcano #1. Air Saturated Sea Water (ASSW) is also reported for comparison. The ^{3}He concentration and R/Ra values are also plotted vs the sampling depth.

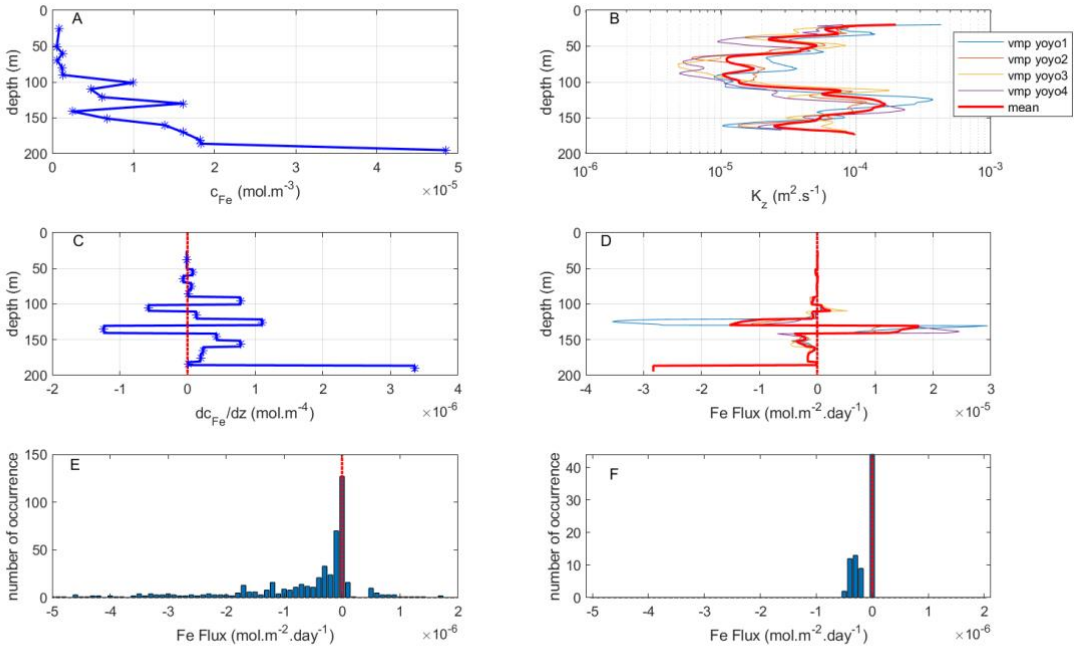

Fig. S2. Station above Volcano #1 (A) Dissolved Fe (DFe) concentrations, C_{Fe} (B) Vertical eddy diffusivity, Kz (C) Vertical gradient of DFe, dc_{Fe}/dz. (D) DFe turbulent diffusive flux, in red, the mean flux. (E) Histogram of DFe turbulent diffusive flux for the whole profile. (F) Same as (E) but at the base of the mixed layer.

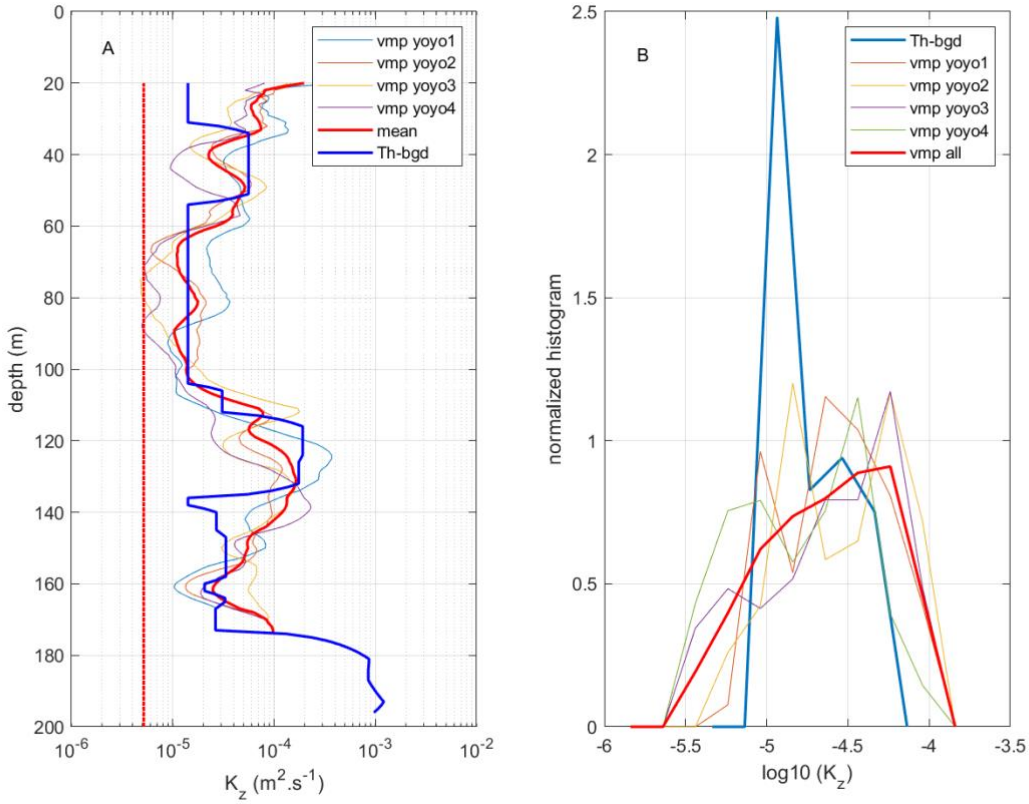

Fig. S3. Validation of the indirect estimate of vertical eddy diffusivity from CTD at Volcano 1: (A) Measured averaged Kz profile at Volcano 1 (red), and estimated Kz from CTD (cyan), individual VMP profiles (thin colored curves). The constant value for a background internal wave far from sources and sinks is shown with a vertical red line. (B) Normalized histograms of vertical eddy diffusivity (log10), indirect estimate from CTD (blue), all VMP data (red), individual profiles (thin colored curves).

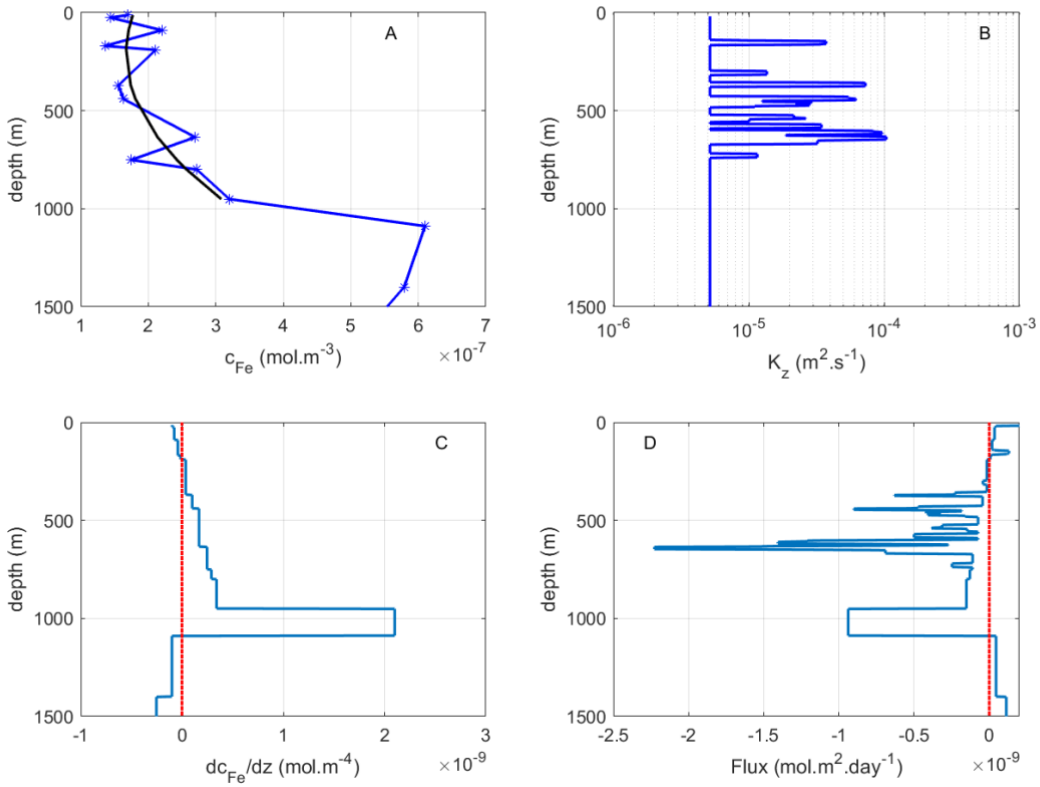

Fig. S4. Reference site (gyre) (A) Dissolved iron concentrations, c_{Fe} (B) Vertical eddy diffusivity estimate, Kz, (C) Vertical gradient of DFe, dc_{Fe}/dz. (D) DFe turbulent diffusive flux.

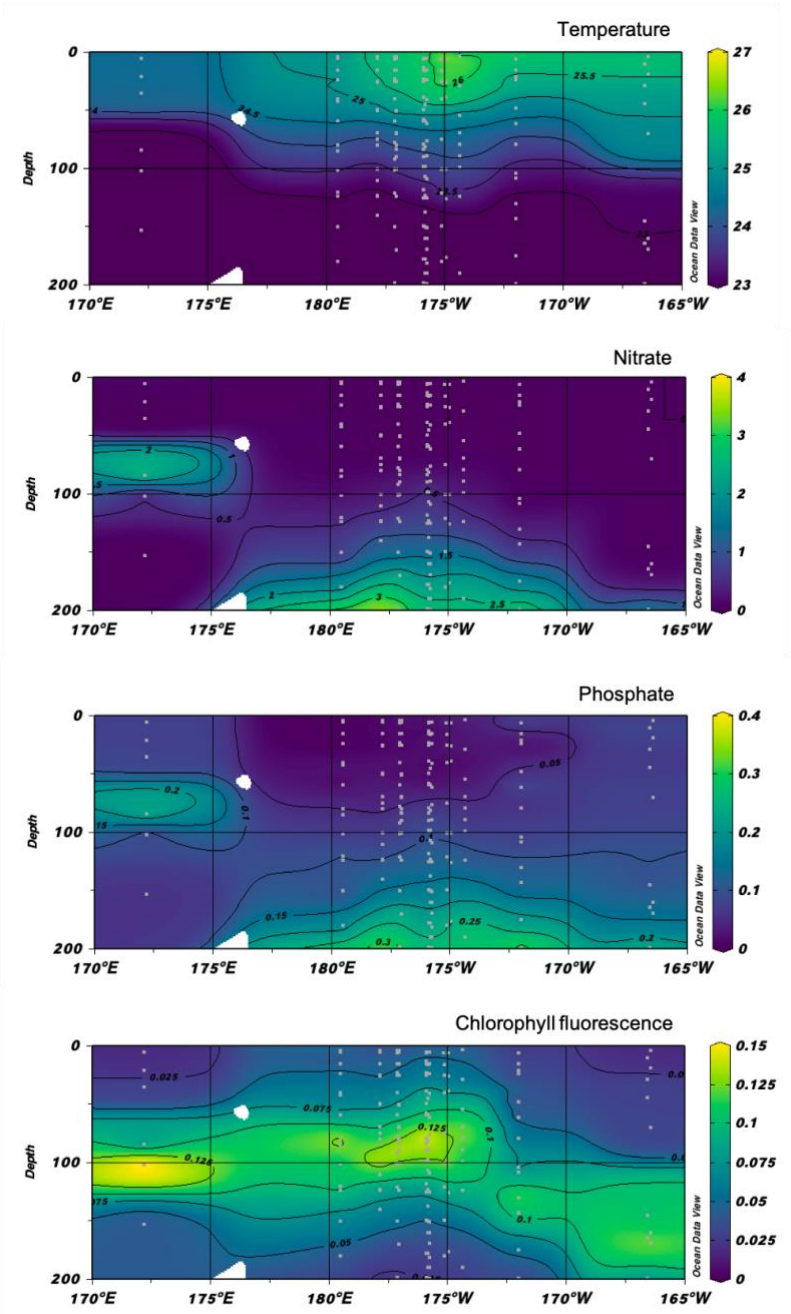

Fig. S5. Horizontal and vertical distributions physico-chemical parameters during the TONGA transect. A. Seawater temperature (°C), B. nitrate concentrations (µmol liter^{-1}), C. phosphate concentrations (µmol liter^{-1}) and D. Chlorophyll Fluorescence, across the TONGA transect. Y axis: pressure (dbar), X axis: longitude; grey dots correspond to sampling depths at the various stations.

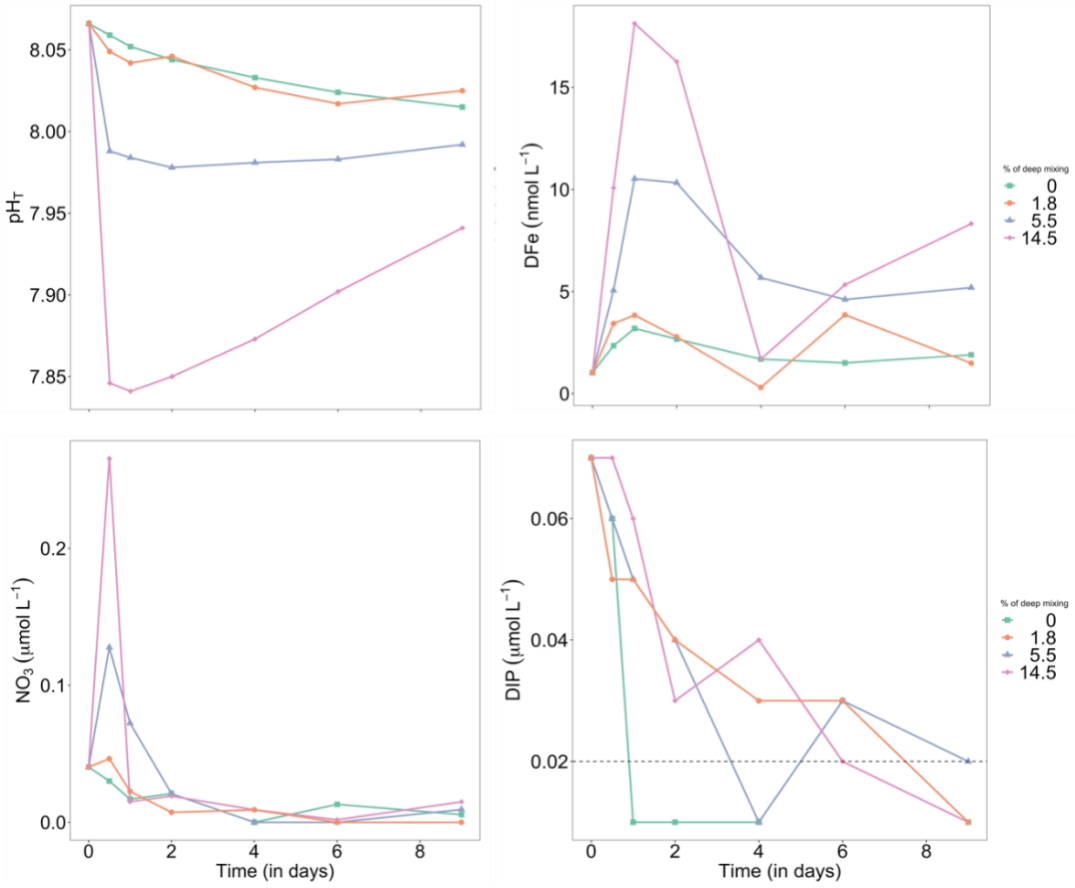

Fig. S6. Temporal evolution of (A) pH, (B) DFe concentrations, (C) Nitrate concentrations, and (D) Dissolved Inorganic Phosphorus (DIP) concentrations during the minicosm experiments. The T0 corresponds to the values measured before mixing in ambient seawater.

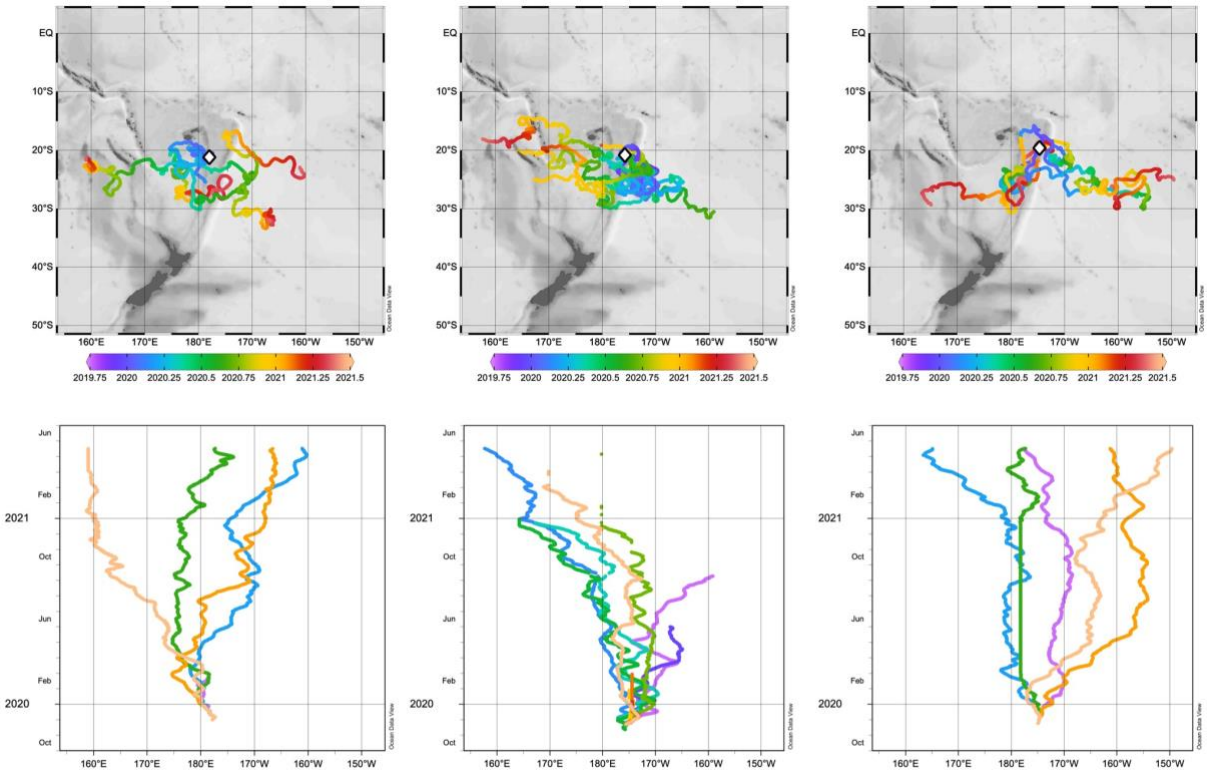

Fig. S7. 20 months trajectories of SVP drifters deployed at Volcano #1 (middle panels) and two adjacent sites in the Lau Basin (left and right panels) during the TONGA cruise. The three clusters of deployment (5 drifters per cluster) are indicated by the white diamonds. Lower panels: zonal dispersion of each cluster during the 20 months.

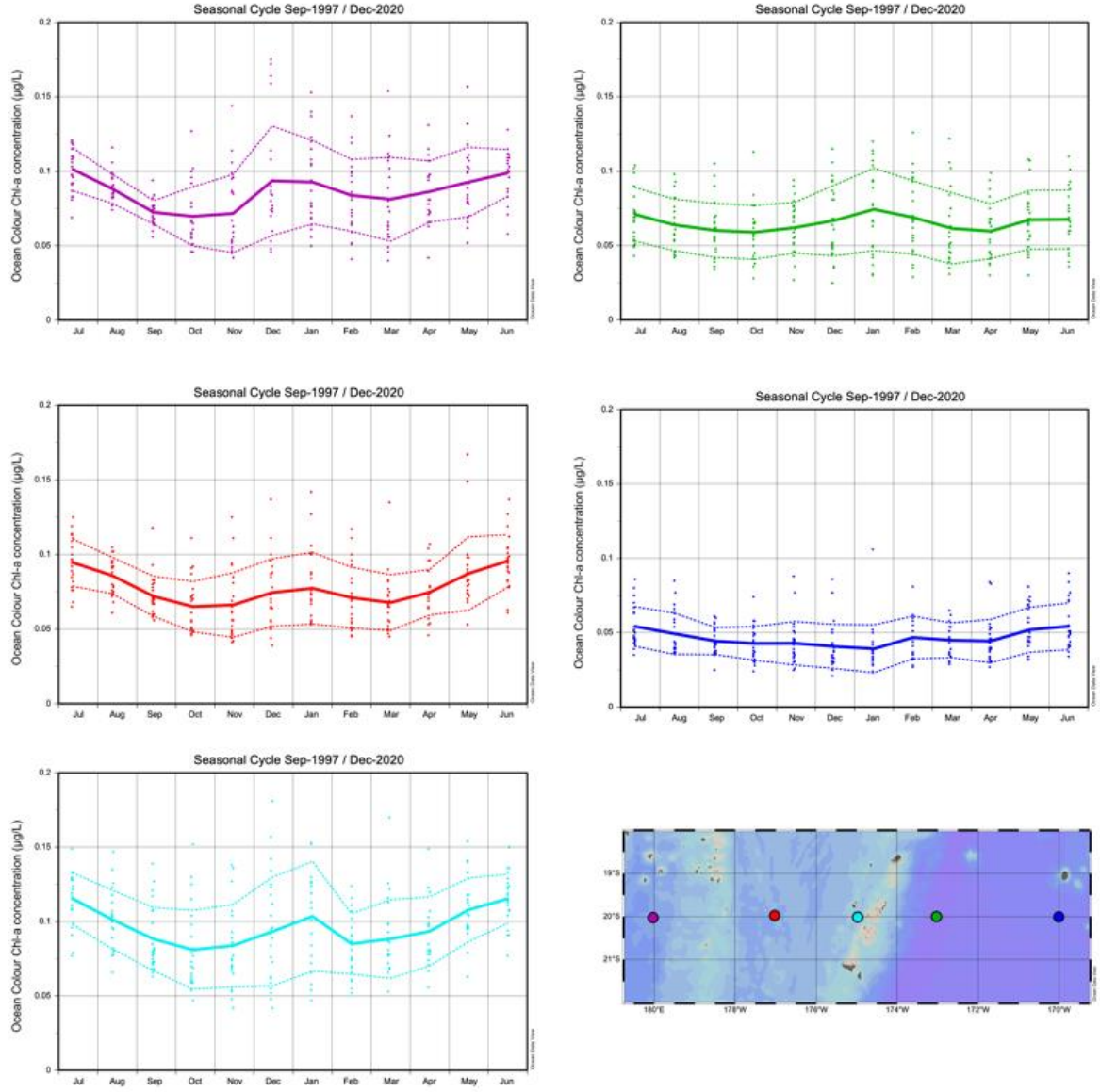

Fig. S8. 23-years time series of chlorophyll-a concentration seasonal cycles in the WTSP. Data are derived from 23-years monthly "cloud free" Copernicus-Globcolour database, at five zonal locations of the TONGA transect. Every values indicated in dots, mean values for each month indicated in bold lines, associated standard deviation in dotted lines.

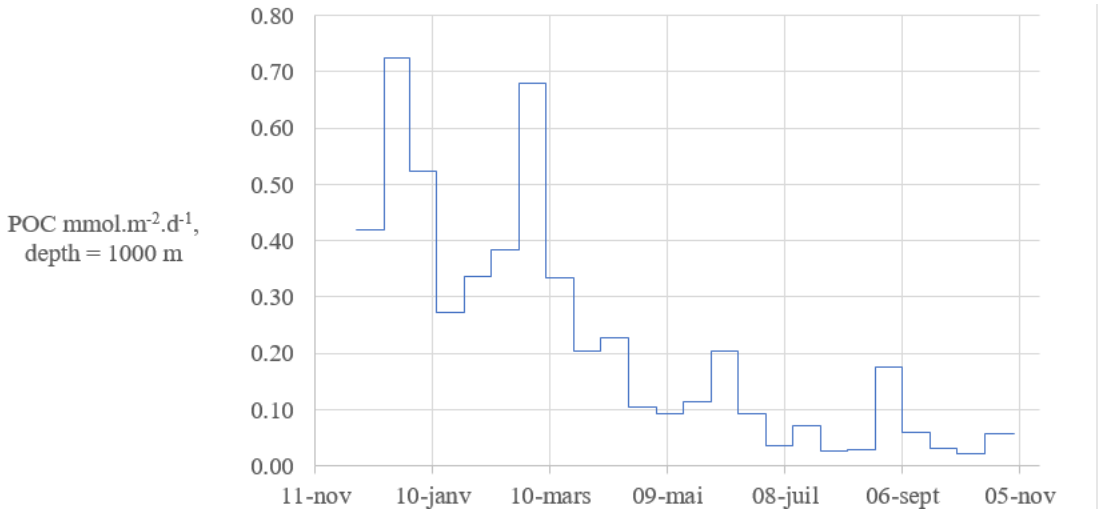

Fig. S9. Particulate organic carbon export fluxes (1000 m) in the Fe-fertilized patch.

Table S1. Mean values and standard deviations of vertical eddy diffusivity, vertical gradient of DFe and turbulent diffusive flux of DFe at the base of the mixed layer (where most biological biomass accumulates) above Volcano #1 and at the reference site. Values in italic of standard deviations are computed over the euphotic layer when no variations at the base of the mixed layer.

Above Volcano #1				**Reference site**		
Depth	Kz $m^2 s^{-1}$	Dc/dz mol m^{-4}	Flux mol $m^{-2} d^{-1}$	Kz $m^2 s^{-1}$	Dc/dz mol m^{-4}	Flux mol $m^{-2} d^{-1}$
40m-60m	$3.68x10^{-5}$ $\pm 1.91x10^{-5}$	$3.12x10^{-8}$ $\pm 4.71x10^{-8}$	$-1.06x10^{-7}$ $\pm 1.68x10^{-7}$	$5.17x10^{-6}$ *$\pm 9.66x10^{-6}$*	$7.75x10^{-11}$ *$\pm 3.08x10^{-11}$*	$3.46x10^{-11}$ *$\pm 3.08x10^{-11}$*

Table S2. Mean values and standard deviations of vertical gradient of nitrate, phosphate and silicate and their turbulent diffusive fluxes at the base of the mixed layer above Volcano #1

Depth	Nitrate Dc/dz mol m^{-4}	Nitrate flux mol $m^{-2} d^{-1}$	Phosphate Dc/dz mol m^{-4}	Phosphate flux mol $m^{-2} d^{-1}$	Silicate Dc/dz- mol m^{-4}	Silicate flux mol $m^{-2} d^{-1}$
40m-60m	0	**0**	$1.60x10^{-6}$ ±0	$-5.43x10^{-6}$ $\pm 2.38x10^{-6}$	$1.20x10^{-6}$±0	$-4.07x10^{-6}$±$1.78x10^{-6}$

1. K. G. Foote, H. P. Knudsen, G. Vestnes, Calibration of Acoustic Instruments for Fish Density-Estimation - a Practical Guide. *J Acoust Soc Am* **83**, 831-832 (1988).
2. Y. Sano, T. P. Fischer, in *The noble gases as geochemical tracers*. (Springer, 2013), pp. 249-317.
3. W. Aeschbach-Hertig, D. K. Solomon, Noble gas thermometry in groundwater hydrology. *The noble gases as geochemical tracers*, 81-122 (2013).
4. A. L. Rizzo *et al.*, Kolumbo submarine volcano (Greece): An active window into the Aegean subduction system. *Scientific Reports* **6**, (2016).
5. C. Guieu *et al.*, Iron from a submarine source impacts the productive layer of the Western Tropical South Pacific (WTSP). *Scientific Reports* **8**, 9075 (2018).
6. M. Tonnard *et al.*, Dissolved iron in the North Atlantic Ocean and Labrador Sea along the GEOVIDE section (GEOTRACES section GA01). *Biogeosciences* **17**, 917-943 (2020).
7. P. Bouruet-Aubertot *et al.*, Longitudinal contrast in turbulence along a similar to 19 degrees S section in the Pacific and its consequences for biogeochemical fluxes. *Biogeosciences* **15**, 7485-7504 (2018).
8. T. R. Osborn, Estimates of the Local-Rate of Vertical Diffusion from Dissipation Measurements. *J Phys Oceanogr* **10**, 83-89 (1980).
9. T. M. Dillon, Vertical Overturns - a Comparison of Thorpe and Ozmidov Length Scales. *J Geophys Res-Oceans* **87**, 9601-9613 (1982).
10. S. A. Thorpe, Turbulence and Mixing in a Scottish Loch. *Philos T R Soc A* **286**, 125-181 (1977).
11. E. Kunze, E. Firing, J. M. Hummon, T. K. Chereskin, A. M. Thurnherr, Global abyssal mixing inferred from lowered ADCP shear and CTD strain profiles (vol 36, pg 1553, 2006). *J Phys Oceanogr* **36**, 2350-2352 (2006).
12. A. Aminot, R. Kerouel, Quae, Ed. (2007), pp. 187 pp.
13. S. Bonnet *et al.*, In-depth characterization of diazotroph activity across the western tropical South Pacific hotspot of N-2 fixation (OUTPACE cruise). *Biogeosciences* **15**, 4215-4232 (2018).
14. I. Klawonn *et al.*, Simple approach for the preparation of 15−15N2-enriched water for nitrogen fixation assessments: evaluation, application and recommendations. *Frontiers in microbiology* **6**, (2015).
15. M. Benavides, H. Berthelot, S. Duhamel, P. Raimbault, S. Bonnet, Dissolved organic matter uptake by Trichodesmium in the Southwest Pacific. *Scientific Reports* **7**, 41315 (2017).
16. P. H. Moisander *et al.*, Analogous nutrient limitations in unicellular diazotrophs and *Prochlorococcus* in the South Pacific Ocean. *The ISME journal* **6**, 733-744 (2011).
17. J. P. Montoya, M. Voss, P. Kahler, D. G. Capone, A simple, high-precision, high-sensitivity tracer assay for N_2 fixation. *Applied and Environmental Microbiology* **62**, 986-993 (1996).
18. T. M. Kana *et al.*, A membrane inlet mass spectrometer for rapid high precision determination of N_2, O_2, and Ar in environmental water samples. *Analytical Chemistry* **66**, 4166–4170 (1994).
19. A. M. Moisander, A. Beinart, M. Voss, J. P. Zehr, Diversity and abundance of diazotrophs in the South China Sea during intermonsoon. *The ISME journal* **2**, 954-967 (2008).
20. M. J. Church, B. D. Jenkins, D. M. Karl, J. P. Zehr, Vertical distributions of nitrogen-fixing phylotypes at Stn ALOHA in the oligotrophic North Pacific Ocean. *Aquatic Microbial Ecology* **38**, 3-14 (2005).

21. K. A. Turk-Kubo *et al.*, Diazotroph community succession during the VAHINE mesocosms experiment (New Caledonia Lagoon). *Biogeosciences* **12**, 7435-7452 (2015).
22. P. W. Boyd, A. McDonnell, J. Valdez, D. LeFevre, M. P. Gall, RESPIRE: An in situ particle interceptor to conduct particle remineralization and microbial dynamics studies in the oceans' Twilight Zone. *Limnol Oceanogr-Meth* **13**, 494-508 (2015).
23. M. Bressac *et al.*, Resupply of mesopelagic dissolved iron controlled by particulate iron composition. *Nature Geoscience* **12**, 995-+ (2019).
24. L. A. Anderson, J. L. Sarmiento, Redfield Ratios of Remineralization Determined by Nutrient Data-Analysis. *Global Biogeochemical Cycles* **8**, 65-80 (1994).
25. C. Guieu *et al.*, Vertical particle flux in the northeast Atlantic Ocean (POMME experiment). *J Geophys Res-Oceans* **110**, (2005).
26. K. L. Casciotti, D. M. Sigman, M. G. Hastings, J. K. Böhlke, A. Hilkert, Measurement of the Oxygen Isotopic Composition of Nitrate in Seawater and Freshwater Using the Denitrifier Method. *Analytical Chemistry* **74**, 4905–4912 (2002).
27. D. M. Sigman *et al.*, A bacterial method for the nitrogen isotopic analysis of nitrate in seawater and freshwater. *Analytical Chemistry* **73**, 4145–4153 (2001).
28. M. R. McIlvin, K. L. Casciotti, Technical updates to the bacterial method for nitrate isotopic analyses. *Analytical Chemistry* **83**, 1850-1856 (2011).
29. F. Gazeau *et al.*, Impact of dust addition on the metabolism of Mediterranean plankton communities and carbon export under present and future conditions of pH and temperature. *Biogeosciences* **18**, 5423-5446 (2021).